Geometric and Topological Approaches to Shape Variation in *Ginkgo* Leaves

Luke Mander[1], Martin Bauer[2], Haibin Hang[3], Washington Mio[2]

[1]School of Environment, Earth and Ecosystem Sciences, The Open University, Milton Keynes, MK7 6AA, UK; [2]Department of Mathematics, Florida State University, Tallahassee, FL 32306, USA; [3]Department of Mathematical Sciences, University of Delaware, Newark, DE 19716, USA

Author for correspondence:
Luke Mander
Email: luke.mander@gmail.com

Abstract

Leaf shape is a key plant trait that varies enormously. The diversity of leaf shape, and the range of applications for data on this trait, requires frequent methodological developments so that researchers have an up-to-date toolkit with which to quantify leaf shape. We generated a dataset of 468 leaves produced by *Ginkgo biloba*, and 24 fossil leaves produced by evolutionary relatives of extant *Ginkgo*. We quantified the shape of each leaf by developing a geometric method based on elastic curves and a topological method based on persistent homology. Our geometric method indicates that shape variation in modern leaves is dominated by leaf size, furrow depth, and the angle of the two lobes at the base of the leaf that is also related to leaf width. Our topological method indicates that shape variation in modern leaves is dominated by leaf size and furrow depth. Both methods indicate that there is greater diversity in the shape of fossil leaves compared to modern leaves. The two approaches we have described can be applied to modern and fossil material, and are complementary: identifying similar primary patterns of variation, but revealing some different aspects of morphological variation.

Key words: Morphometric methods, elastic curves, persistent homology, biological shape, plant traits.

Introduction

Leaf shape is a fascinatingly diverse plant trait. It can vary between taxa, between individuals in different populations of the same species, and for some species there are striking variations in leaf shape within a single plant, a phenomenon known as heterophylly. Additionally, different regions of a leaf expand at different rates during development, and this leads to allometric changes in shape as a leaf grows. Leaves are primary sites of photosynthesis and play a central role in the growth and survival of a plant, and work has shown that variation in leaf shape may be related to thermoregulation, the constraints of hydraulics and mechanics, patterns of leaf expansion, as well as the avoidance of herbivory and the optimal interception of light (Nicotra *et al.*, 2011). Leaf shape is therefore a trait for which there are many functional trade-offs, and from an ecological perspective may be viewed "not as a single major axis, but rather as an option that fine tunes the leaf to its conditions over both short and evolutionary time spans" (Nicotra *et al.*, 2011, p. 547).

The taxonomic and ecological significance of leaf shape has led to the development of numerous methods to characterize this trait. Certain methods rely on largely qualitative observation. For example, aspects of leaf shape can be described using specialist terminology (Leaf Architecture Working Group 1999), which allows leaves to be placed into categories based on their gross morphology, and this approach has proved useful in studies of plant architecture (e.g. Leigh, 1999; Barthelemy & Caraglio, 2007) and studies of fossil leaves that may not be preserved in their entirety (e.g. Johnson, 1992). Other methods for characterising leaf shape are based on morphometric measurements of certain features on a leaf, which can either be made manually by human researchers or computationally using image analysis software. For example, Leigh *et al.* (2011) described leaf shape using measurements of leaf area and leaf dissection (leaf perimeter/area) in the context of plant hydraulics, and Royer *et al.* (2005) used the same measure of leaf dissection to investigate the relationship between mean annual temperature and leaf shape. Measurements of such morphological features are often used to generate indices of leaf shape, such as compactness ($perimeter^2/area$) and shape factor (4π x leaf area/$perimeter^2$), which are used to summarize aspects of leaf shape and show how it relates to the environment

or has changed through time (Royer *et al.*, 2008, 2009; Bacon *et al.*, 2013). Morphometric techniques that use landmarks (a constellation of discrete anatomical loci, each described by 2- or 3-dimensional Cartesian coordinates (Webster & Sheets, 2010)) to quantify morphology have also been employed to capture variation in leaf shape (Weight *et al.*, 2008), and have highlighted differing developmental and evolutionary contributions to leaf shape (Chitwood *et al.*, 2016). Persistent homology—a topological data analysis method—has also been applied to the problem of quantifying leaf shape (Li *et al.*, 2018a,b), and represents a morphometric framework to measure plant form that allows comparison of the morphology of different plant organs such as leaves, roots and stems (Bucksch *et al.*, 2017; Li *et al.*, 2017).

Owing to the diversity of leaf form—and the range of applications for data on leaf morphology—regular methodological experimentation is required so that researchers have an up-to-date toolkit with which to quantify this key plant trait. In this paper, we provide such experimentation through a quantitative morphological study of the leaves of *Ginkgo biloba* L., an extant gymnosperm that is noted for the diversity of leaf shapes that are produced by individual specimens (e.g. Leigh *et al.*, 2011). *Ginkgo* has a long evolutionary history and extinct relatives of this plant were important elements of Earth's vegetation during the Mesozoic Era (~250–65 million years ago). Fossil leaves of plants that are evolutionary ancestors of living *Ginkgo* are commonly found in sedimentary rocks, and our study includes a small number (24) of such fossil leaves.

We do not initially focus on any specific morphological features such as leaf length or the nature of the leaf margin. Instead, we take an exploratory approach to the morphology of *Ginkgo* leaves, using geometric and topological methods to reveal the features that explain the observed variation in leaf shape. Our specific aims are as follows: (1) to develop a geometric method and a topological method for quantifying leaf shape; (2) to apply these methods to the leaves of living *Ginkgo* in order to reveal which features explain the observed variation in the shape of sampled leaves; (3) to compare the results produced by the two methods in order to explore the degree to which they reveal different aspects of morphological variation; and (4) to apply our methods to fossil leaves

of ancient evolutionary relatives of living *Ginkgo* in order to demonstrate how they could be used to study the evolution of leaf shape through geological time.

A Dataset of Modern and Fossil Leaves

Mature and fully expanded leaves were harvested from a *Ginkgo biloba* tree growing as a specimen on the campus of The Open University, UK. The specimen is reproductively immature and was ascended using a ladder. Seven branches from approximately halfway up the specimen were removed from the trunk using a saw. Every leaf growing on each branch was plucked from the base of the petiole and dried in a plant press. A total of 468 leaves from a mixture of short-shoots and long-shoots were collected from the specimen. Each of these leaves was photographed next to a scale bar using a digital camera positioned 20cm above a light box. Twenty-two fossil leaves produced by evolutionary relatives of living *Ginkgo biloba* were extracted from the collections of the Natural History Museum in London, and two fossil leaves were extracted from the geology collections of the School of Environment, Earth and Ecosystem Sciences, The Open University (Table 1). Each fossil leaf was photographed next to a scale bar using a digital camera and the outline of each fossil was traced using Adobe Illustrator to create a digital outline of each leaf. The petioles of fossil leaves are frequently broken, distorted or completely absent as a result of the fossilization process. A central goal of our manuscript is to compare living and fossil *Ginkgo* leaves and in order to facilitate this, we have excluded the petiole from our analyses. Our analyses are therefore focussed on the shape of *Ginkgo* leaf blades. Our dataset of modern and fossil *Ginkgo* leaf images is available in the Supplementary Information.

A Geometric Approach to Quantifying the Shape of Leaves

Methods

We represented each *Ginkgo* leaf blade by its boundary curve, with values mapped in the plane (two dimensional Euclidean space) (Fig. 1). When considering these representations of *Ginkgo* leaves we factored out the actions of rotation and translation and reparameterization. For example, two identical leaves could each be represented by their boundary curves, but each curve could

be considered distinct from one another if they differed only by rotation (a curve could be presented at 90 degrees on top of the other for instance), but our analysis factors out such actions. It is possible to also factor out the action of scaling in analyses of this nature, however, since leaf size is relevant to our study we do not factor out scaling.

To quantitatively model morphological variation in our sample of *Ginkgo* leaves, we introduce a similarity measure for shapes that serves as the basis of statistical analysis. This is an intricate process for two main reasons: (1) the infinite dimensionality of the ensemble of all shapes; and (2) the non-linearity of shape space. To overcome this difficulty, we appeal to the concepts of Riemannian geometry, and use a Riemannian metric that quantifies the difficulty of morphing one boundary curve onto another by measuring the geodesic distance between the curves, accounting for rotations, translations and reparameterizations. This enables us to quantify shape similarity as the minimal deformation cost to reshape a curve, in this case a *Ginkgo* leaf contour. Despite the nonlinear nature of shape space, this framework allows us to calculate mean shapes and locally linearize shape data about the mean, which, in turn, lets us employ standard statistical methods on linearized data to analyse the shape variation present in our sample of *Ginkgo* leaves.

The Riemannian metric we employ is grounded on principles of linear elasticity and is formally defined on the ensemble of parametric curves, but its invariance properties ensure that it descends to a shape metric. A precise definition of the metric and a discussion of its main properties may be found in Bauer *et al.* (2017, 2019) (see also Klassen *et al*. (2004) for related shape metrics). In practice, the comparison of *Ginkgo* leaf boundary curves is a shape-matching problem, and to solve it we discretized the boundary curve of each leaf using a B-spline representation with 100 control points. This reduces the problem of comparing leaf boundary curves to a finite-dimensional optimization problem that can be solved with standard methods of numerical optimization. We use principal component analysis (PCA) to uncover the principal modes of shape variation in *Ginkgo* leaves.

Results

We calculated the Karcher mean of our sample of modern *Ginkgo* leaves (Fig. 1) and then locally linearized the data about the mean in order to uncover the principal modes of leaf shape variation. This was accomplished by solving a shape-matching problem between the mean and each leaf in the dataset. Principal component analysis on the linearized data indicated that approximately 30 components are needed to explain 80% of the shape variation in our sample of *Ginkgo* leaves (Fig. 2a), and we graphically display the first five modes of leaf shape variation using geodesic PCA plots (Fig. 2b–f). The first mode is leaf size (first principal component, Fig. 2b), the second and third modes are the depth of the furrow that separates the two lobes of the typical *Ginkgo* leaf, together with the angle of the two lobes at the base of the leaf that is also related to leaf width (second principal component, Fig. 2c). Some leaves, for example, have a very deep furrow whereas others have no furrow at all. Similarly, some leaves have lobes that are quite pointed and curve backwards towards the leaf base, whereas others have lobes that do not curve backwards. The interpretation of higher principal components is less clear. The third principal component might be connected to a shift in the lateral position of the furrow (Fig. 3d), and the fourth and fifth principal components may relate to the small indentations and crenulations on leaf margins (Fig. 2e,f).

Examples of variability in terms of the three primary morphological features identified by our geodesic plots (Fig. 2b,c) can be seen in a PCA ordination of our dataset of *Ginkgo* leaves (Fig. 3). Leaves towards the top are relatively small and leaves towards the base are relatively large (Fig. 3). Leaves to the left are typically characterized by a small or absent furrow, and/or lobes that do not curve backwards, leaves to the right are typically characterized by a furrow and/or pointed lobes that slightly curve backwards towards the leaf base (Fig. 3). This plot also highlights that the morphological space occupied by our sample of *Ginkgo* leaves, as delineated by our geometric approach, is organized as a single cloud. Most data points are concentrated towards the center of the ordination, and the distribution of data points becomes sparser with increasing distance from the center (Fig. 3).

A Topological Approach to Quantifying the Shape of Leaves

231 ***Methods***

232 We employed the topological data analysis technique persistent homology (PH)
233 (Edelsbrunner & Harer 2010; Otter *et al*. 2017; Li *et al*. 2018a,b) and represented
234 each *Ginkgo* leaf in our dataset with a persistence barcode. To construct this
235 barcode, for each point on the contour of a leaf, we calculated the distance to the
236 point *P* where the leaf blade meets the petiole (Fig. 4a). Distance was measured
237 in pixels and in our source images 152 pixels = 1 cm. All images were
238 downscaled by 1/8 and so 19 pixels = 1 cm in our analyses. For each $r > 0$, we
239 counted the number of connected components formed by the points on the
240 contour whose distance to *P* is greater or equal to *r* and recorded this count as a
241 barcode. For example, for $r = 8.6$, there are 4 connected components (these are
242 the uninterrupted segments of the leaf blade contour, Fig. 4a), so there are $b = 4$
243 bars over that value of *r* (Fig. 4b). Similarly, for $r = 7.0, 5.4, 3.8$, (Fig. 4a) the
244 corresponding number of bars is b = 3, 2, 1 (Fig. 4b). The barcode summarizes
245 the count as we gradually lower the threshold r, with bars disappearing as
246 connected components coalesce and bars appearing as new components emerge.
247 The coalescence of two connected components follows the elder rule: the first-
248 born bar survives while the younger bar dies. Through this construct, we
249 mapped the dataset of leaves to a dataset of barcodes, with each leaf described
250 by a barcode. In order to facilitate statistical analysis, we vectorized each
251 barcode by listing the length of the bars in decreasing order. Since different
252 leaves may produce barcodes with different number of bars, we padded the tails
253 of the vectors with zeros to make all vectors the same length. In our analysis of
254 modern leaves, statistical analyses were performed on these padded vectors. In
255 our analysis of modern and fossil *Ginkgo* leaves combined, statistical analyses
256 were performed on vectors that were normalized by the length of the first bar
257 (the first component of each normalized vector was therefore 1 and discarded).
258

259 ***Results***

260 Figure 5 shows the results of PCA applied to the vectorized barcode data. The
261 first PC explains approximately 75% of the total variance and inspection of the
262 PC loadings indicates that it is dominated by leaf length, followed by furrow
263 depth. The second PC explains about 22% of the total variance mainly as

variation in the depth of the furrow, followed by (negative) variation in leaf length. This ordination indicates that the morphological space occupied by our sample of *Ginkgo* leaves, as delineated by our topological approach, is organized as a single cloud, although the leaves with PC1 scores < 0 and PC2 scores > 15 are somewhat separated from the other leaves in our sample (Fig. 5). To facilitate visualization of shape variation among our sample of *Ginkgo* leaves, the original leaf images corresponding to two discrete paths, nearly parallel to the first two principal PC axes, are highlighted in Fig. 5. These two paths show contrasting behaviour: PC1 captures a pattern in which larger leaves have a deeper furrow, whereas PC2 captures a pattern in which smaller leaves have a deeper furrow.

Application to Fossil *Ginkgo* Leaves

Visual inspection of fossil leaf boundary curves highlights that the diversity of leaf shapes in our collection of *Ginkgo* fossils is greater than that found in our sample of modern *Ginkgo* leaves (compare Fig. 1 and Fig. 6a, see also the Supplementary Information). In particular, several fossil leaves are characterised by multiple deep furrows so that leaf blades consist of multiple lobes rather than just two as in the typical *Ginkgo biloba* leaf, while other fossils have highly dissected leaf margins. This greater diversity in fossil leaf shapes is picked up by both the geometric and the topological approaches we have described, and both indicate that there are fossil leaves situated outside the total range of morphological space occupied by modern *Ginkgo* leaves (Fig. 6b,c). Both approaches also highlight that there are some fossils leaves that are very similar to modern *Ginkgo* leaves, and there are some fossil and modern leaves that overlap in morphological space (Fig. 6b,c).

However, there are differences in the degree to which modern and fossil leaves are separated in morphological space using our two approaches. Using our geometric approach, relatively small leaves with shapes characterised by multiple lobes lie outside the morphological space occupied by modern *Ginkgo* leaves, while relatively large leaves with highly dissected margins plot within the space occupied by modern leaves (Fig. 6b). In contrast, using our topological approach, both of these types of fossil leaves plot outside the morphological space occupied by modern *Ginkgo* leaves (Fig. 6c). Our topological approach very

clearly captures similarities and differences between modern and fossil leaves that are expected on the basis of their visual appearance alone (Fig. 6c), whereas using our geometric approach the distinction between modern and fossil leaves is not as clear (Fig. 6b).

Discussion

Comparison of Approaches

The two approaches we have described in this paper measure leaf shape in different ways: our geometric approach is based on analysing boundary curves with an elastic metric (Fig. 2), whereas our topological approach is based on measuring the number of connected components as a leaf is partitioned into different segments (Fig. 4). Despite these differences, the two approaches both indicate that leaf size and the nature of the furrow separating the two lobes of a typical *Ginkgo* leaf are primary features that explain the observed variation in leaf shape. Both approaches also distinguish the leaves of *Ginkgo* long shoots from those of short shoots. The leaves of long shoots are typically smaller and can have a deep wide furrow and a dissected margin, while the leaves of short shoots are typically larger and can have a less pronounced furrow (Leigh *et al.*, 2011). These two leaf types also have different structural and hydraulic properties, probably related to greater hydraulic limitation of long-shoot leaves during leaf expansion (Leigh *et al.*, 2011). In the PCA summary of our geometric approach, the long shoot leaves are situated to the top left of the plot with low PC1 scores and high PC2 scores, and form a sparsely occupied region of morphological space (Fig. 3). In the PCA summary of our topological approach, the long shoot leaves are situated in the top left of the plot with low PC1 scores and high PC2 scores, and form a sparsely occupied region of *Ginkgo* leaf morphospace (Fig. 5).

There are also certain differences in the morphological features pinpointed by each approach. For example, our geometric approach suggests that the angle of the two lobes at the base of the leaf (also related to leaf width) is an important mode of morphological variation in the population of leaves we have studied (Fig. 2c), but this aspect of leaf morphology is not clearly picked up by our topological approach (Fig. 5). Additionally, our topological approach is

able to quantify the nature of the indentations in the leaf margin more clearly than our geometric approach. This is because our topological features, by design, precisely measure the depth of indentations—from large furrows to minor crenulations—in the leaf margin. The vectors we used in our topological analysis of modern and fossil *Ginkgo* leaves were normalized by the length of the first bar, and each vector therefore encodes the depths of the various indentations in the leaf margin relative to absolute leaf size ordered from deep to shallow. This is highlighted in the horizontal transect in Figure 6d: to the left are modern and fossil *Ginkgo* leaves that lack indentations, whereas to the right are leaves with increasingly complex indentations, but the size of each leaf in each highlighted group varies considerably. In the language of descriptive botany, the MDS axes highlight types of leaf dissection, with axis one representing a gradient from no dissection (low axis one scores) to many relatively deep indentations (high axis one score) (Fig. 6d), and axis two representing a gradient from few relatively deep indentations (low axis two scores) to many relatively shallow indentations (high axis two scores) (Fig. 6c). This morphological feature may only be recorded in the higher orders of variation in our geometric approach (fourth and fifth principal components for our modern *Ginkgo* leaves, see Fig. 2e,f). The two approaches we have described are therefore complementary, identifying similar primary patterns of variation, but also revealing some different aspects of morphological variation.

From the perspective of PH applied to the problem of quantifying leaf shape, previous approaches have been based on measurements of the Euler characteristic curve (Li *et al.*, 2018a,b). Our approach is different in that we have constructed a persistence barcode from a count of connected components formed by points on a contour at incremental distances from the base of a leaf blade (Fig. 4), and this demonstrates an alternative means by which PH can quantify leaf shape. Oftentimes, a challenge in the use of PH is the interpretation of a persistence barcode (e.g. Otter *et al.*, 2017), but for the barcodes we have generated here, the length of the longest bar represents the largest distance to *P* (Fig. 4) and is therefore a quantifier of leaf size, while the next longest bar relates to the depth of the furrow in a *Ginkgo* leaf that displays this trait, and other smaller bars relate to the depth of smaller indentations in the leaf margin. The

363 statistical interpretation of persistence barcodes is also challenging, and as noted
364 by Otter *et al*. (2017, p. 3) for example, "the space of barcodes lacks geometric
365 properties that would make it easy to define basic concepts such as mean,
366 median, and so on". In contrast, the framework of our geometric approach allows
367 for the calculation of mean shapes and the linearization of data around the mean,
368 and this highlights the complementary nature of the two approaches to leaf
369 shape we have described in this paper.
370
371 ***Looking Ahead: Image Segmentation, Fossils and Future Applications***
372 Image segmentation—the partitioning of a digital image into multiple
373 segments—is a key step in any study involving the computational analysis of
374 digital imagery. In this study, the goal of image segmentation was to represent
375 each leaf by its outline. For our sample of modern *Ginkgo* leaves we were able to
376 achieve segmentation computationally because the leaves themselves were
377 whole, free from damage such as indentations in the leaf margin, and the images
378 were free from major defects such as blurring. However, for the fossil *Ginkgo*
379 leaves we have analysed, segmentation involved tracing the outline of each fossil
380 leaf by hand rather than delineating the leaf margin computationally. Such
381 manual tracing has been used in the segmentation and analysis of images of leaf
382 venation networks (Blonder *et al*., 2019, 2020), and in the context of fossil
383 leaves, this hand-tracing approach allows the analyst to manually join small
384 areas of the leaf margin that have been fragmented by the fossilization process
385 or damaged during the extraction or storage of the specimen.
386 In some cases of damage to a specimen, the original undamaged margin of
387 a leaf was extremely faint, sometimes only visible using a microscope, whereas in
388 others the leaf margin was interrupted by a scratch or hidden by a small piece of
389 sediment (see the Supplementary Information). In situations such as these,
390 knowledge of the processes leading to the formation and preservation of fossil
391 leaves was used to calibrate a restoration of the fossil outline to what was judged
392 to be its original state. This process introduces a source of potential error that is
393 not quantified, and future work could explore how to automate elements of this
394 image segmentation step, perhaps using a library of fossil leaf outlines produced
395 by manual tracing to train a classifier, or perhaps repairing defects in the leaf

margin computationally using techniques from inpainting (see Bertalmio *et al*., 2000). The latter could be particularly valuable in studies of leaves where damage by insects is high such as in lowland moist tropical rainforests.

The inclusion of fossil leaves in this exploratory analysis (Fig. 6) indicates that both the PH framework and geometric methods based on elastic curves have potential application to evolutionary and palaeoecological problems that require data on leaf shape in the geological past (e.g. Johnson, 1992; Leaf Architecture Working Group, 1999; Royer *et al*., 2008, 2009; Bacon *et al.*, 2013). Shape data derived from these approaches could also be used as classifiers in machine learning work to automate the classification of leaves in studies of modern and ancient plant diversity (cf. Wilf *et al.*, 2016), and could help quantify the nature and rate of leaf shape change during development. The methods we have described could also be used to quantify other planar shapes produced by plants such as the sepals, petals, and tepals of flowers, which may enhance studies of the relationship between morphology and pollination biology (cf. Mander *et al.*, 2020)

Acknowledgements

We are grateful to Peta Hayes for assistance with locating, accessing, and photographing fossil *Ginkgo* leaves in the collections of the Natural History Museum, London. WM acknowledges NSF grant DMS-1722995, MB was partially supported by NSF grant DMS-1953244.

References

Bacon KL, Belcher CM, Haworth M, McElwain JC. 2013. Increased Atmospheric SO2 Detected from Changes in Leaf Physiognomy across the Triassic–Jurassic Boundary Interval of East Greenland. *PloS ONE* **8**: e60614.

Barthelemy D, Caraglio Y. 2007. Plant Architecture: A Dynamic, Multilevel and Comprehensive Approach to Plant Form, Structure and Ontogeny. *Annals of Botany* **99**: 375–407.

Bauer M, Bruveris M, Harms P, Møller-Andersen J. 2017. A numerical framework for Sobolev metrics on the space of curves. *SIAM Journal on Imaging Sciences* **10**: 47-73.

Bauer M, Bruveris M, Charon , Møller-Andersen J. 2019. A relaxed approach for curve matching with elastic metrics. *ESAIM: Control, Optimisation and Calculus of Variations* **25**: 72.

Bertalmio M, Sapiro G, Caselles V, Ballester C. 2000. Image inpainting. *SIGGRAPH '00: Proceedings of the 27th Annual Conference on Computer Graphics and Interactive Techniques* 417–424.

Blonder B, Both S, Jodra M, Majalop N, Burslem DFRP, Teh YA, Malhi Y. 2019. Leaf venation networks of Bornean trees: images and hand-traced segmentations. *Ecology* **100**: e02844.

Blonder B, Both S, Jodra M, Xu H, Fricker M, Matos IS, Majalop N, Burslem DFRP, Teh YA, Malhi Y. 2020. Linking functional traits to multiscale statistics of leaf venation networks. *New Phytologist* Early View.

Bucksch A, Atta-Boateng A, Azihou AF, Battogtokh D, Baumgartner A, Binder BM, Braybrook SA, Chang C, Coneva V et al. 2017. Morphological Plant Modeling: Unleashing Geometric and Topological Potential within the Plant Sciences. *Frontiers in Plant Science* **8**: 900.

Chitwood DH, Klein LL, O'Hanlon R, Chacko S, Greg M, Kitchen C, Miller AJ, Londo JP. 2016. Latent developmental and evolutionary shapes embedded within the grapevine leaf. *New Phytologist* **210**: 343–355.

Johnson KR. 1992. Leaf-fossil evidence for extensive floral extinction at the Cretaceous-Tertiary boundary, North Dakota, USA. *Cretaceous Research* **13**: 91–117.

Klassen E, Srivastava A, Mio M, Joshi SH. 2004. Analysis of planar shapes using geodesic paths on shape spaces. *IEEE transactions on pattern analysis and machine intelligence* **26**: 372-383.

Leaf Architecture Working Group. 1999. Manual of Leaf Architecture - morphological description and categorization of dicotyledonous and net-veined monocotyledonous angiosperms. 65p.

Leigh A, Zwieniecki MA, Rockwell FE, Boyce CK, Nicotra AB, Holbrook NM. 2011. Structural and physiological correlates of heterophylly in *Ginkgo biloba* L. *New Phytologist* **189**: 459–470.

Leigh EG. Jr. 1999. *Tropical Forest Ecology*. Oxford University Press, New York.

Li M, Duncan K, Topp CN, Chitwood DH. 2017. Persistent homology and the branching topologies of plants. *American Journal of Botany* **104**: 349–353.

Li M, Frank MH, Coneva V, Mio W, Chitwood DH, Topp CN. 2018a. The persistent homology mathematical framework provides enhanced genotype-to-phenotype associations for plant morphology. *Plant Physiology* **177**: 1382–1395.

Li M, An H, Angelovici R, Bagaza C, Batushansky A, Clark L, Coneva V, Donoghue M, Edwards E et al. 2018b. Topological data analysis as a morphometric method: using persistent homology to demarcate a leaf morphospace. *Frontiers in Plant Science* **9**: 553.

Mander L, Parins-Fukuchi C, Dick CW, Punyasena SW, Jaramillo C. 2020. Phylogenetic and ecological correlates of pollen morphological diversity in a Neotropical reainforest. *Biotropica* Early View.

Nicotra AB, Leigh A, Boyce CK, Jones CS, Niklas KJ, Royer DL, Tsukaya H. 2011. The evolution and functional significance of leaf shape in the angiosperms. *Functional Plant Biology* **38**: 535–552.

Otter N, Porter MA, Tillmann U, Grindrod P, Harington HA. 2017. A roadmap for the computation of persistent homology. *EPJ Data Science* **6**: 17.

Royer DL, Wilf P, Janesko DA, Kowalski EA, Dilcher DL. 2005. Correlations of climate and plant ecology to leaf size and shape: Potential proxies for the fossil record. *American Journal of Botany* **92**: 1141–1152.

Royer D, McElwain J, Adams J. 2008. Sensitivity of leaf size and shape to climate within Acer rubrum and Quercus kelloggii. *New Phytologist* **179**: 808–817.

Royer DL, Meyerson LA, Robertson KM, Adams JM. 2009. Phenotypic plasticity of leaf shape along a temperature gradient in Acer rubrum. *PloS ONE* **4**: e7653.

Webster M, Sheets HD. 2010. A practical introduction to landmark-based morphometrics. *Paleontological Society Special Papers* **16**: 163–188.

Weight C, Parnham D, Waites R. 2008. LeafAnalyser: a computational method for rapid and large-scale analyses of leaf shape variation. *Plant Journal* **53**: 578–586.

Wilf P, Zhang S, Chikkerur S, Little SA, Wing SL, Serre T. 2016. Computer vision cracks the leaf code. *Proceeding of the national Academy of Sciences, USA* **113**: 3305–3310.

Supplementary Information

A dataset of modern and fossil *Ginkgo* leaf images.

Fig. and Table captions

Fig. 1. Collection of all 468 *Ginkgo biloba* leaves in our dataset represented by their boundary curves (black lines) with the Karcher mean leaf shape superimposed (red line).

Fig. 2. Geodesic PCA plots of *Ginkgo* leaves represented in the tangent space of the mean. Variance explained by each principal component (a), first principle component (b), second principle component (c), third principle component (d), fourth principle component (e), fifth principle component (f).

Fig. 3. PCA ordination scatterplot (PC1 on horizontal axis, PC2 on vertical axis) showing the morphological variation among 468 modern *Ginkgo* leaves that is revealed by our geometric approach to leaf shape.

Fig. 4. Schematic example showing the construction of a persistence barcode that describes the shape of a *Ginkgo* leaf. Four distances from the point *P* where the leaf blade meets the petiole are shown: r = 8.6, 7.0, 5.4, 3.8 (a). At the distance r = 8.6, there are four connected components outside the dashed line (a). At the distance r = 7.0, there are three connected components, at r = 5.4 there are two (the two lobes of the typical *Ginkgo* leaf), while at r = 3.8 there is one uninterrupted segment of the leaf blade contour outside the dashed line (a). To construct a barcode that represents a leaf, we do not count the number of connected components at widely spaced intervals as shown in (a). Instead, we perform a count for each $r > 0$, and record the number of connected components as r is gradually lowered in a barcode (b).

Fig. 5. PCA ordination scatterplot (PC1 on horizontal axis, PC2 on vertical axis) showing the morphological variation among 468 modern *Ginkgo* leaves that is revealed by our topological (PH) approach to leaf shape. Nine leaves from the PC1 pathway (red) and nine leaves from the PC2 pathway (blue) are shown to highlight modes of morphological variation (all leaves displayed at the same scale).

Fig. 6. Collection of 24 fossil *Ginkgo* leaves, each represented by their boundary curves (a). PCA ordination scatterplot (PC1 on horizontal axis, PC2 on vertical axis) showing morphological variation of modern *Ginkgo* leaves (black datapoints) together with fossil *Ginkgo* leaves (red datapoints) based on our geometric approach, the PCs together explain 64% of the variation (b). MDS ordination showing morphological variation of modern *Ginkgo* leaves together with fossil *Ginkgo* leaves based on our topological approach, with a vertical transect of enlarged leaves highlighted in blue (c) and a vertical transect of enlarged leaves highlighted in blue (d). Modern leaves displayed with black datapoints and fossil leaves displayed with red datapoints (b–d).

558 **Table 1.** Fossil *Ginkgo* leaves housed in the collections of the Natural History
559 Museum, London, and The Open University that we have investigated in this
560 paper.
561

Specimen Name	Accession Number	Age	Country	Location	Specimen Number (This Study)
Ginkgo cranei	NHM: V.68763	Paleocene	United States	North Dakota	fossil_1
Ginkgo cranei	NHM: V.68764	Paleocene	United States	North Dakota	fossil_2
Ginkgo gardneri	NHM: V.14834	Eocene	Scotland	Isle of Mull	fossil_3
Ginkgo gardneri	NHM: V.14838	Paleocene/Eocene	Scotland	Isle of Mull	fossil_4
Ginkgo gardneri	NHM: V.18436	Eocene	Scotland	Isle of Mull	fossil_5
Ginkgo gardneri	NHM: V.24999	Eocene	Scotland	Isle of Mull	fossil_6
Ginkgo sp.	NHM: V.2477	Eocene	Scotland	Isle of Mull	fossil_7
Ginkgo digitata	NHM: V.24587	Cretaceous	Australia	Queensland	fossil_8
Ginkgo digitata	NHM: V.39211	Jurassic	England	Yorkshire	fossil_9
Ginkgo digitata	NHM: V.13503	Jurassic	England	Yorkshire	fossil_10
Ginkgo digitata	NHM: V.10316	Jurassic	England	Yorkshire	fossil_11
Ginkgo huttonii	NHM: V.60195	Jurassic	England	Yorkshire	fossil_12
Ginkgo huttonii	NHM: V.3580	Jurassic	England	Yorkshire	fossil_13
Ginkgo huttonii	NHM: V.40511	Jurassic	England	Yorkshire	fossil_14
Ginkgo huttonii	NHM: V.39210	Jurassic	England	Yorkshire	fossil_15
Ginkgo huttonii	NHM: V.978	Jurassic	England	Yorkshire	fossil_16
Ginkgo huttonii	NHM: V.979	Jurassic	England	Yorkshire	fossil_17
Ginkgo longifolius	NHM: V.39209	Jurassic	England	Yorkshire	fossil_18
Ginkgo siberica	NHM: V.58618	Jurassic	England	Yorkshire	fossil_19
Ginkgo digitata	NHM: V.3423	Jurassic	England	Gloucestershire	fossil_20
Ginkgo digitata	NHM: V.3429	Jurassic	England	Gloucestershire	fossil_21
Ginkgo siberica	NHM: V.19238	Jurassic	Russia	Irkutsk	fossil_22
Ginkgo huttonii	Open University geology collection	Jurassic	England	Yorkshire	fossil_23
Ginkgo huttonii	Open University geology collection	Jurassic	England	Yorkshire	fossil_24

562

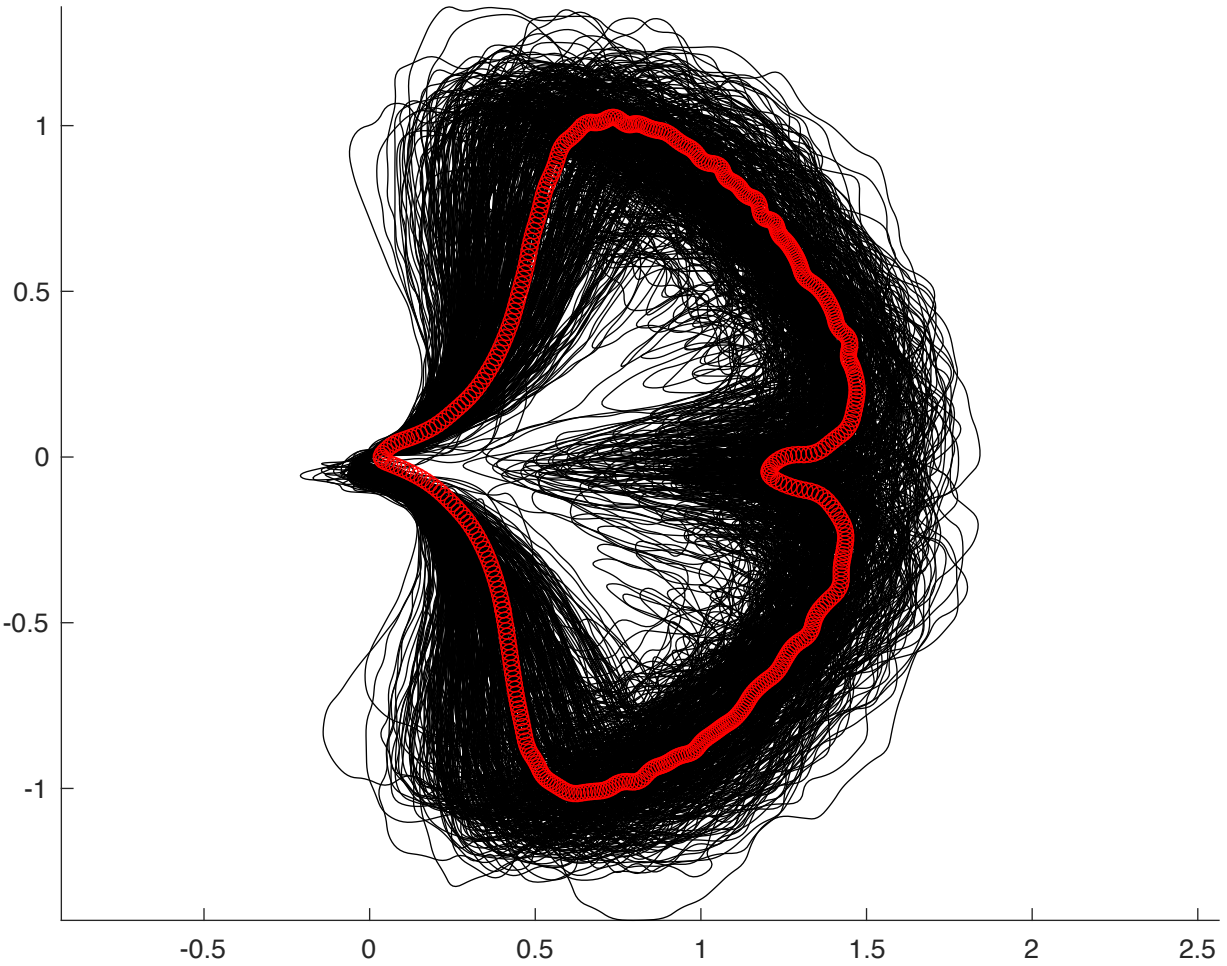
1
0.5
0
-0.5
-1
-0.5
0
0.5
1
1.5
2
2.5

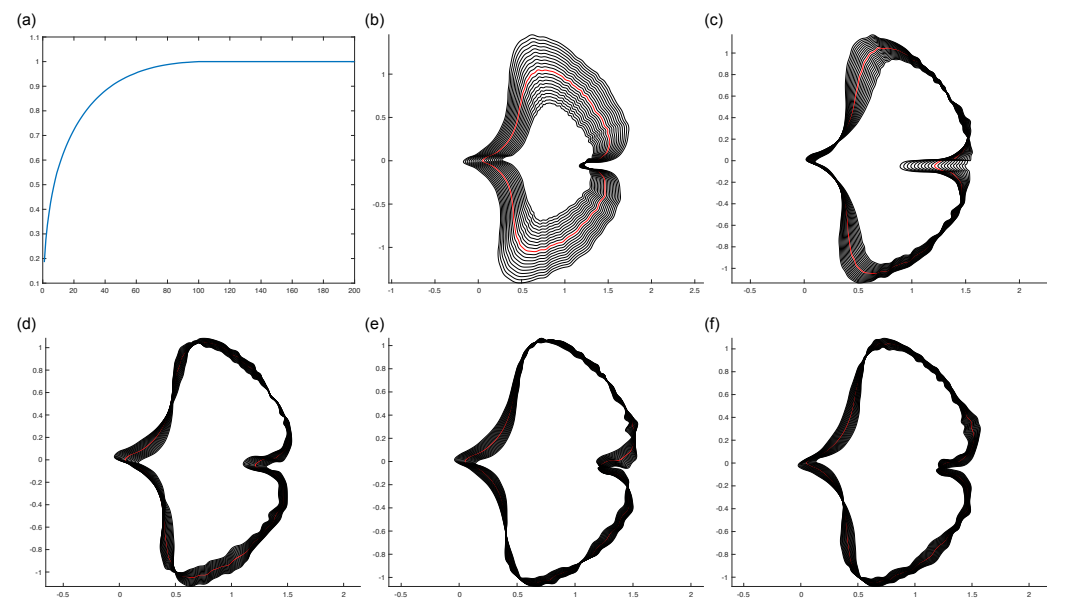
(a)
(b)
(c)
(d)
(e)
(f)

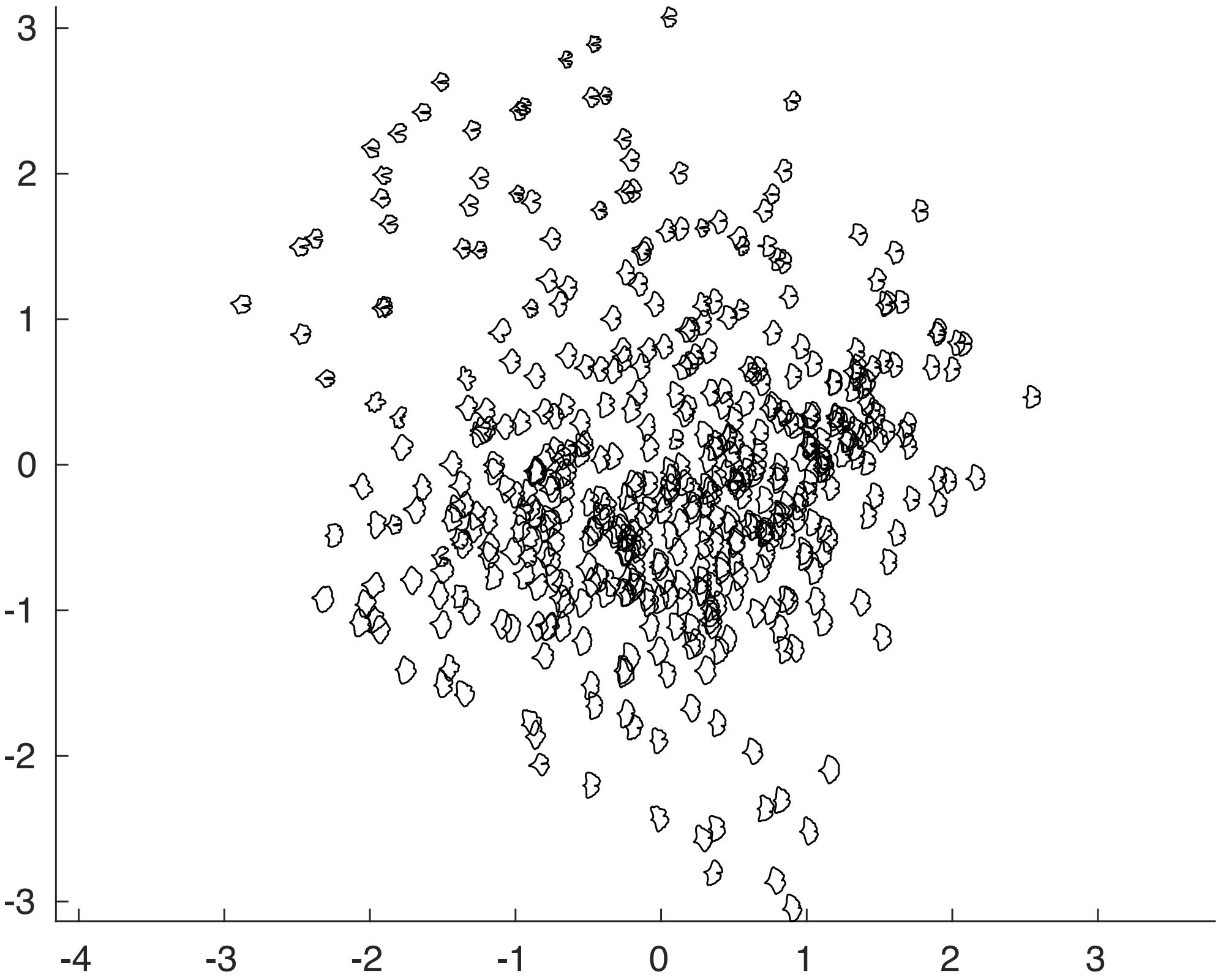
3
2
1
0
-1
-2
-3
-4
-3
-2
-1
0
1
2
3

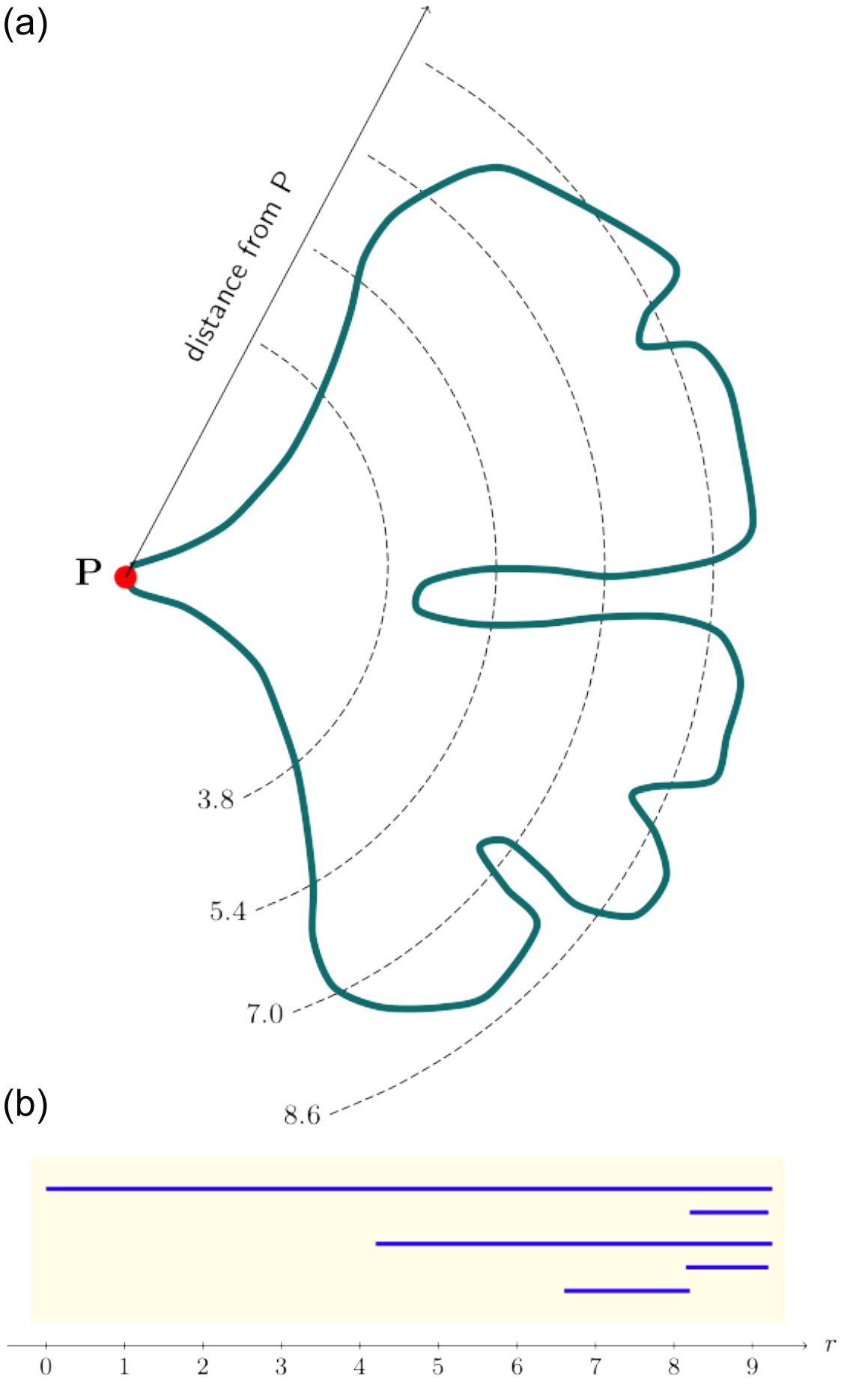
(a)
distance from P
P
3.8
5.4
7.0
8.6
(b)
0
1
2
3
4
5
6
7
8
9
r

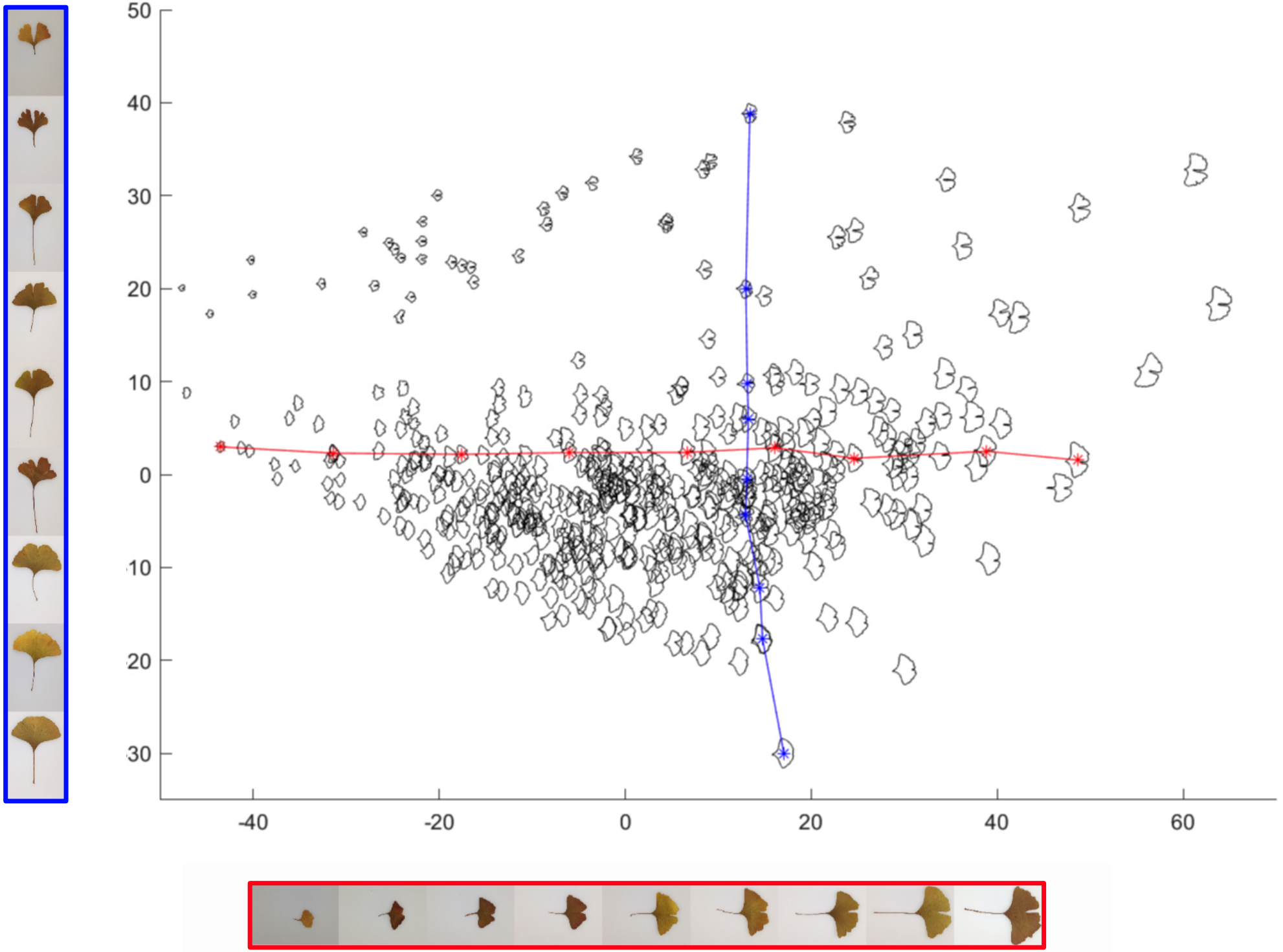
50
40
30
20
10
0
10
20
30
-40
-20
0
20
40
60

(a)

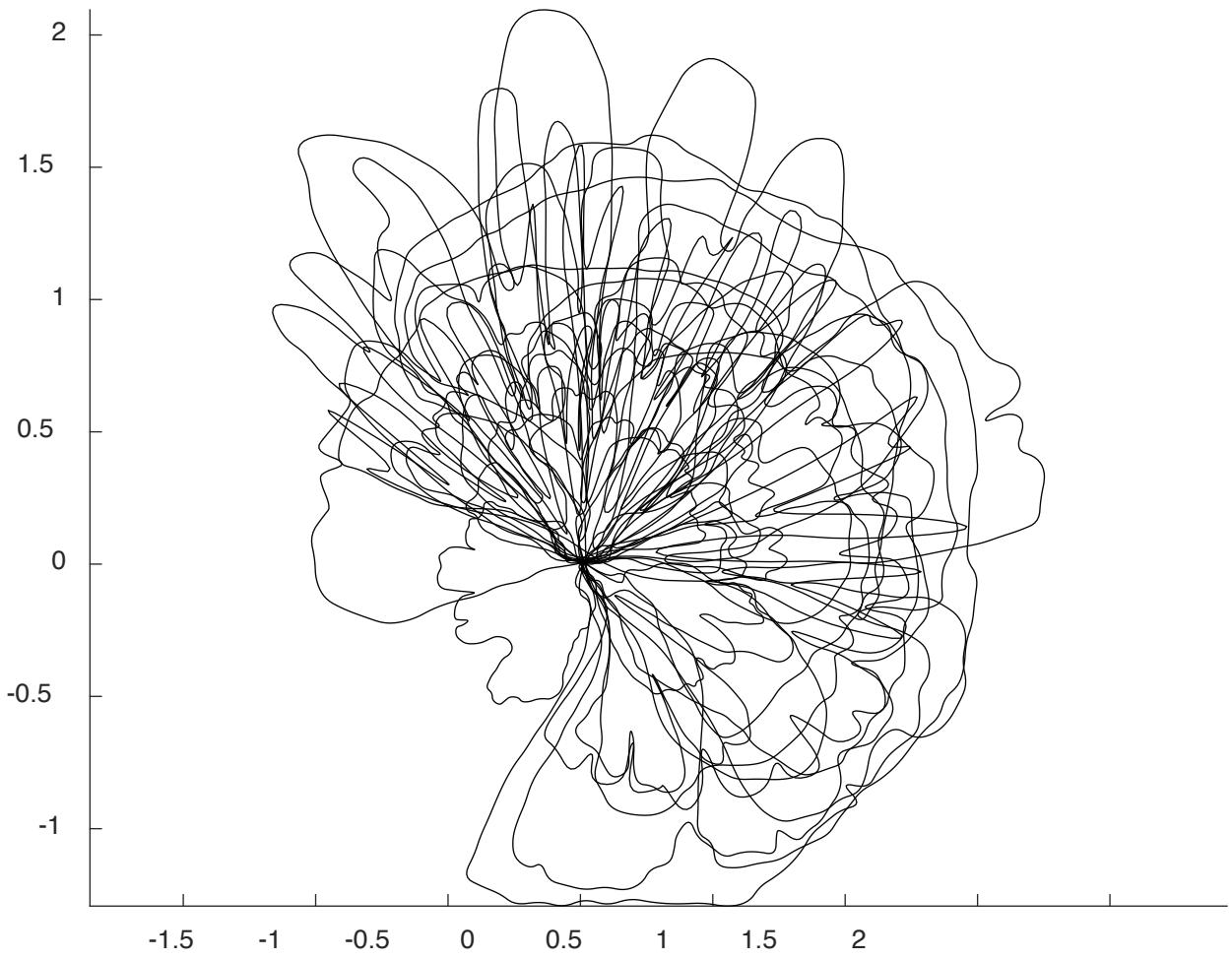

(b)

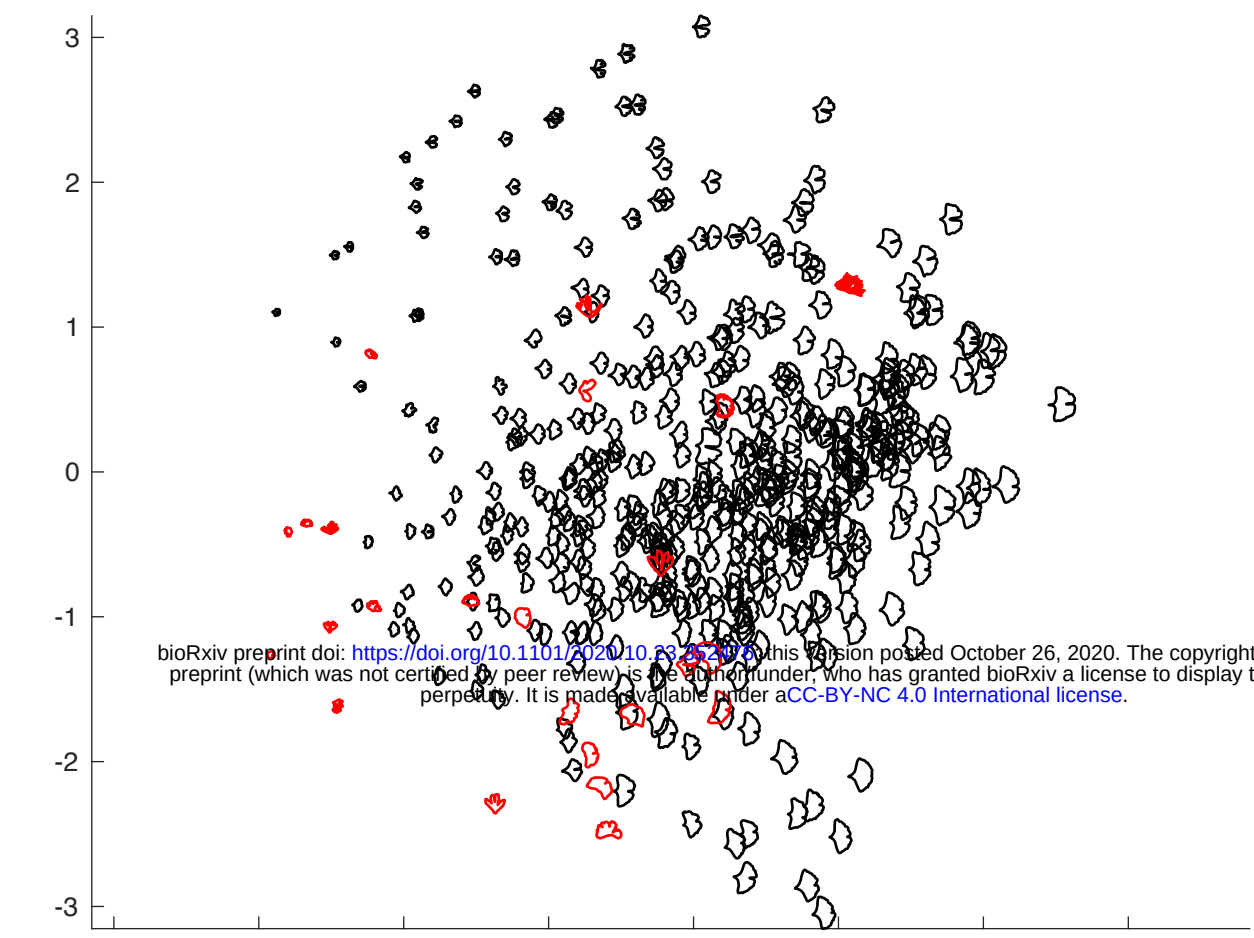

(c)

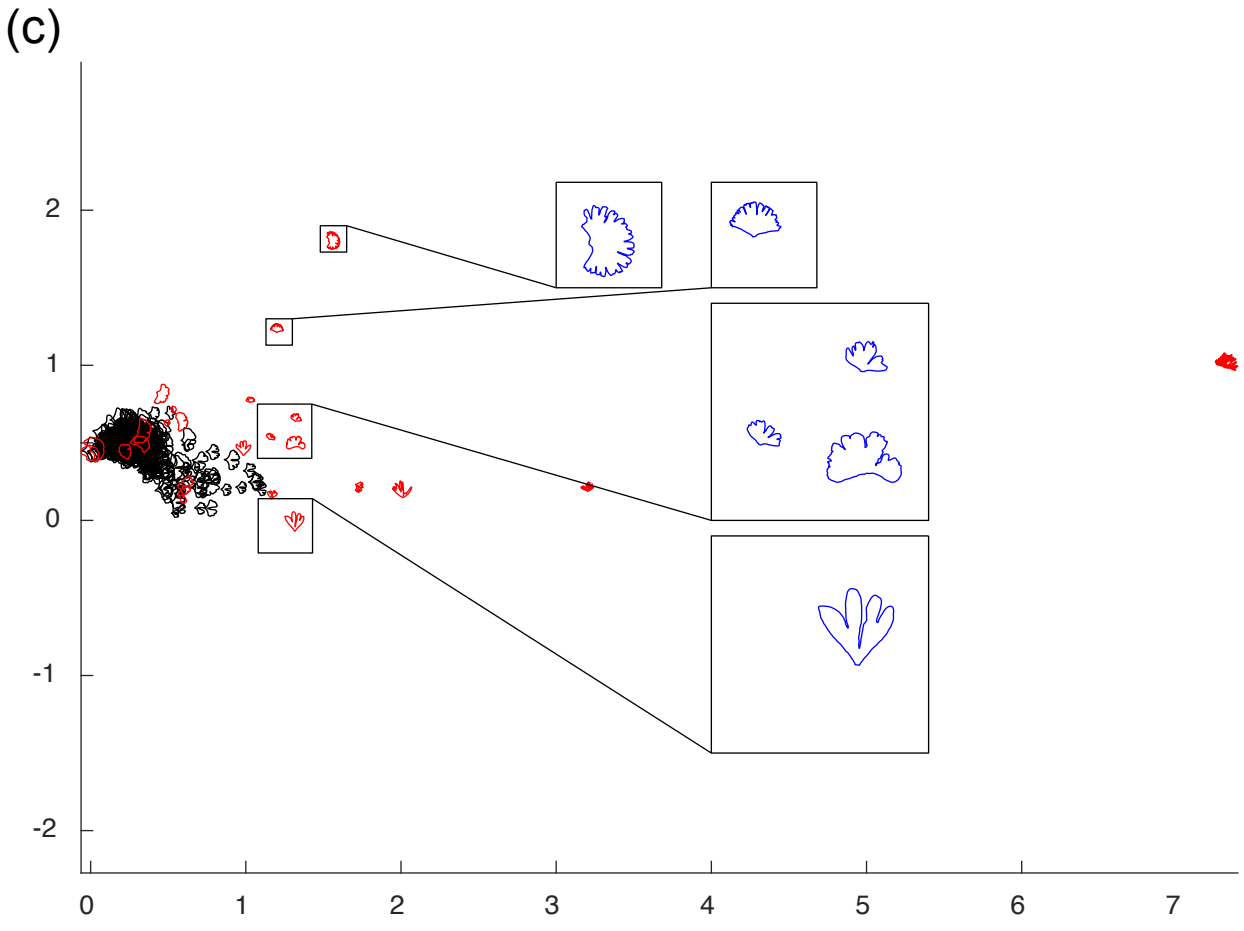

(d)